Available online at www.sciencedirect.com
SciVerse ScienceDirect
Acta Materialia 61 (2013) 3233–3241
Acta MATERIALIA
www.elsevier.com/locate/actamat

Plasticity of bcc micropillars controlled by competition between dislocation multiplication and depletion

Ill Ryu [a,*], William D. Nix [a], Wei Cai [b]

[a] Department of Materials Science and Engineering, Stanford University, Stanford, CA 94305-4040, USA
[b] Department of Mechanical Engineering, Stanford University, Stanford, CA 94305-4040, USA

Received 21 August 2012; received in revised form 9 January 2013; accepted 4 February 2013
Available online 13 March 2013

Abstract

Recent micropillar experiments have shown strong size effects at small pillar diameters. This "smaller is stronger" phenomenon is widely believed to involve dislocation motion, which can be studied using dislocation dynamics (DD) simulations. In the present paper, we use a three-dimensional DD model to study the collective dislocation behavior in body-centered cubic micropillars under compression. Following the molecular dynamics (MD) simulations of Weinberger and Cai, we consider a surface-controlled cross-slip process, involving image forces and non-planar core structures, that leads to multiplication without the presence of artificial dislocation sources or pinning points. The simulations exhibit size effects and effects of initial dislocation density and strain rate on strength, which appear to be in good agreement with recent experimental results and with a simple dislocation kinetics model described here. In addition, at the high strain rates considered, plasticity is governed mainly by the kinetics of dislocation motion, not their elastic interactions.

Keywords: Plasticity; Micropillars; Dislocation dynamics; Stress–strain relations

1. Introduction

As the technology of microscale devices evolves to smaller dimensions, plasticity at small scales is attracting increasing attention. This is driven by the knowledge that many mechanical properties at the sub-micron scale differ from those at the continuum scale. From recent micropillar compression experiments [1–3], it is now known that the flow stress of metallic micropillars increases with decreasing sample size even in the absence of significant hardening by geometrically necessary dislocations or strain gradients [4,5]. Recent review articles have summarized the current state of this research [6,7]. To understand the "smaller is stronger" phenomenon in metals, several models have been proposed, most notably the dislocation starvation model [2,8,9] and the single-arm source model [10–12]. In the dislocation starvation model, the small number of mobile dislocations present in sub-micron pillars is expected to annihilate at the nearby free surfaces during plastic flow, so that nucleation of new dislocations is required for further plastic deformation to occur. In general, higher stresses are required for dislocation nucleation than for activating existing dislocation sources. Since dislocations in smaller pillars might move out of the sample more quickly than they multiply, smaller samples are expected to have higher flow stresses. Recent in situ transmission electron microscopy (TEM) observations of Ni pillars under compression show that mechanical annealing can occur in sub-micron-sized pillars [9]. In the single-arm source model, the radius of the truncated Frank–Read source is smaller in smaller samples, so that the stress needed to activate the source is higher. As a result, smaller samples are predicted to have higher flow stresses. Support for the single-arm source model can be found in the in situ TEM observations [13,14].

* Corresponding author. Present address: 496 Lomita Mall, Durand Bldg., Rm. 129, Stanford University, Stanford, CA 94305, USA. Tel.: +1 650 714 0731; fax: +1 650 725 4034.
E-mail address: iryu@stanford.edu (I. Ryu).

1359-6454/$36.00
http://dx.doi.org/10.1016/j.actamat.2013.02.011

Although in situ TEM is a powerful tool for exploring the microscopic behavior of materials directly, it has several limitations. For example, it requires a very thin electron-transparent section of material and the dislocations often move too fast to be observed clearly [15]. To contribute to a better understanding of small-scale plasticity, it helps to delve more deeply into the details of dislocation behavior, as dislocation motion is the primary mechanism for plastic deformation. In this sense, dislocation dynamics (DD) simulation provides a unique opportunity to explore the motion of individual dislocations, and allows us to develop a better microscopic understanding of the mechanical behavior of micropillars [16–18].

For metals with the face-centered cubic (fcc) crystal structure, DD simulations have provided significant insight into understanding the mechanical behavior at small scales in terms of the collective behavior of dislocations [12,19–24]. The same approach can be taken for body-centered cubic (bcc) metals, provided changes are made to account for the different dislocation mobilities and multiplication mechanisms. For bcc metals, dislocation plasticity is thought to be governed mainly by the motion of screw dislocations, which have a low mobility, attributed to a non-planar core structure and a high Peierls barrier [25–28]. In addition, from molecular dynamics (MD) simulations of plasticity of bcc nanopillars, multiplication is expected to occur by a process of surface induced cross-slip, wherein isolated screw dislocations, aided by image stresses, can self-multiply and generate sources of dislocations [29,30].

In this paper, we implement an algorithm that accounts for surface cross-slip in bcc metal pillars under uniaxial loading in DD models and explore its effect on the macroscopic deformation behavior. Moreover, we compare our simulation results with recent experiments, which have shown that mechanical annealing and exhaustion hardening are also possible in bcc metals [31,32]. To better understand the results of these simulations, a simple dislocation kinetics model is developed, based on the competition between surface controlled multiplication and loss of dislocations by glide out of the micropillar. The DD simulation results and the kinetics model show similar effects of sample size and strain rate on the stress–strain curve.

2. Simulation methods

2.1. Three-dimensional dislocation dynamics in a cylinder geometry

The dislocation dynamics simulations were performed using a modified version of ParaDiS, a DD code originally developed at the Lawrence Livermore National Laboratory [18]. In ParaDiS, dislocations are described as straight perfect dislocation segments connected by nodes. Based on the stress fields of the segments and the loading conditions, dislocation movements are computed and updated. In an effort to make the model conform to a micropillar compression experiment, the traction-free surface should be taken into account. Modifications to the ParaDiS code have been made to account for the presence of the cylinder surface [33]. It considers dislocation motion only in the predefined cylinder region and deletes any dislocations outside of this cylinder region. A spectral method has been developed to compute the image stress field in order to satisfy the traction-free boundary condition on the cylinder surface. However, in this work, we include the effect of the image stress only for the surface nodes by specifying image stresses on them, because they play a critical role in the selection of slip planes and the activation of the surface cross-slip multiplication process. We have seen that ignoring the image stress for all other segments does not make a significant qualitative change in the simulations. Using the surface cross-slip algorithm, we performed DD simulations to explore the effects of sample size, initial dislocation density and strain rate on the stress–strain behavior under uniaxial loading.

2.2. Surface cross-slip mechanism

Recently, Weinberger and Cai [29], using MD, found that even a single, isolated screw dislocation in a bcc nanopillar could multiply by a process involving cross-slip near the surface. They found that the image forces on a straight, inclined, screw dislocation act in opposite directions on either end of the dislocation, causing the two ends of the dislocation to move on different slip planes: the primary plane and the cross-slip plane. The pinning point so created serves as an anchoring point on the glide dislocation, which, above a critical stress, can spiral about that point and create multiple dislocations. Here, we develop a simple algorithm to implement surface-induced cross-slip in the ParaDiS cylinder code. For simplicity, we allow for slip to occur only on the $1/2\langle 111\rangle/\{110\}$ type slip systems. Since only screw dislocations can cross-slip, here we consider a pure screw dislocation in the cylinder geometry, as shown in Fig. 1A. The main task is to determine the slip planes of surface nodes. In Fig. 1B, Peach–Koehler forces due to dislocation interaction and external loading are computed for each surface node. In addition, the image forces are specified at the surface nodes. The image forces act to move the surface nodes in opposite directions, as shown in Fig. 1C. This may be understood by noting that dislocations tend to shorten their length to minimize their energy by rotating. By adding up these forces, the slip planes of the surface nodes are chosen so that the projected force is maximum on the chosen slip plane. In Fig. 1D, the slip plane of the front surface node (A) is the $(1\,0\,1)$ plane, while the slip plane of the back node (B) is the $(0\,\bar{1}\,1)$ plane. Initially, the dislocation is on a single slip plane, but it would move on two different slip planes due to the surface cross-slip mechanism. Because of the surface cross-slip, the dislocation would form a cusp with two arms on different slip planes and evolve into a spiral loop. Afterwards, because the edge dislocation segments move much faster than the screw segments, the loop expands mainly by edge

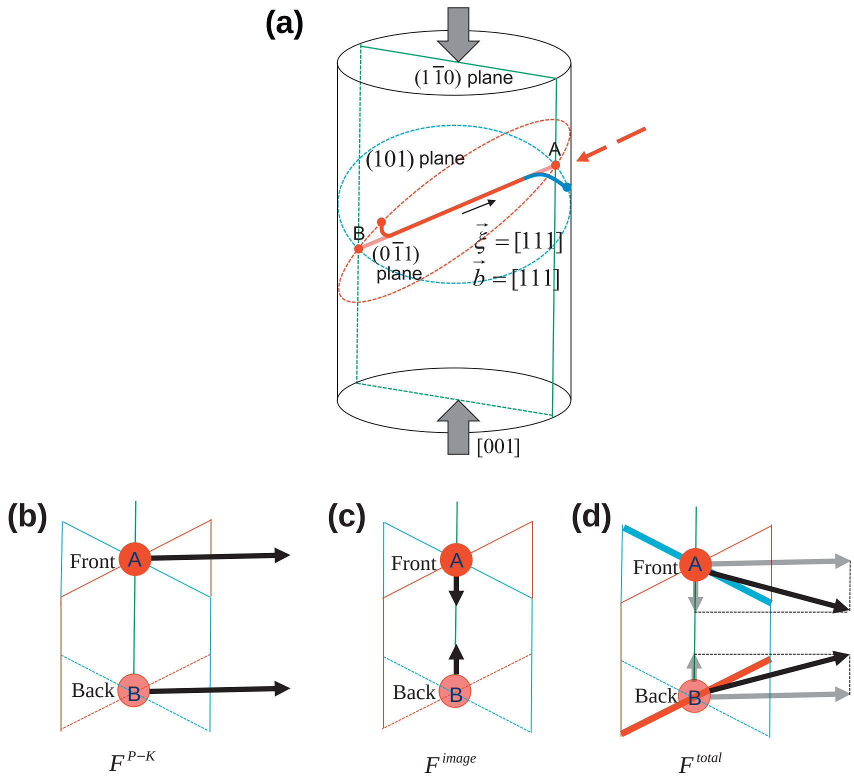

Fig. 1. (a) Single screw dislocation and its slip planes in a cylinder, and (b) Peach–Koehler forces, (c) image forces and (d) total forces on front and back nodes.

motion. For the DD simulation, the mobility of the edge-character segments is set to be 100 times larger than that of the screw segments [29], and dislocation motion is limited to glide in specified slip planes, except for surface dislocation segments. Detailed information on the anisotropic mobility law is given in Ref. [25]. When the edge dislocation segments meet the surface, the one dislocation will have evolved into three dislocations. As a result, a single dislocation can self-multiply (see Supplementary Movie 1A). However, if the stress is lower than a critical stress for a given sized pillar, the cusp will move along the dislocation line and escape from the pillar so that surface multiplication will not occur (see Supplementary Movie 1B). Since the critical stress needed to cause the cusped dislocation to bow and multiply is controlled by an Orowan bowing-like process, the critical stress for multiplication is roughly inversely proportional to the diameter of the pillar.

2.3. Initial dislocation structure

Since the initial dislocation configuration affects the stability of pinning points, it is expected to have a significant effect on the mechanical response of the micropillars [23]. For the modeling of fcc metals, several initial configurations have been suggested: a Frank network relaxed from randomly distributed straight and jogged dislocations [20], randomly distributed Frank–Read sources with pinning points [24] and randomly distributed loops with cross-slip allowed [23]. However, these structures are not especially relevant to bcc metals because of the different edge/screw dislocation mobilities. Moreover, the physical origin of potentially permanent pinning points has remained unknown in sub-micron pillars, based on MD simulations [34].

In the MD study of bcc nanopillars by Weinberger and Cai [29], if a single dislocation is placed in a cylinder, it tends to rotate into a screw orientation to reduce its energy. Because only a few dislocations would exist in sub-micron sized pillars, dislocations would rarely interact with others without external loading. Moreover, since the mobility of the screw orientation is much lower than that of edge, plasticity in bcc micropillars is expected to be governed by screw dislocation motion. As a result, our DD simulation starts with a configuration of randomly distributed pure screw dislocations prior to loading.

3. Simulation results

3.1. Size-dependence of flow stress

To investigate the effect of sample size, simulations were performed with different pillar diameters ranging from 150 nm to 1 μm under periodic boundary conditions along the cylinder axis. For these simulations, a constant axial strain rate of $10^5\ s^{-1}$ was imposed. This is very much higher than typical experimental strain rates of 10^{-3} or $10^{-4}\ s^{-1}$.

Due to time scale limitations, we have not yet been able to model experimental strain rates. The initial dislocation density was $10^{13}\ \mathrm{m}^{-2}$, which amounts to just a few dislocations in the smallest pillars and a much higher line content in the largest pillars. With these conditions, the DD simulation predicts that the stress–strain curve clearly depends on pillar diameter, as shown in Fig. 2. As the sample size decreases from 1 μm to 150 nm in diameter, the flow stress increases from roughly 600 MPa to 1.6 GPa. In addition, smaller samples show "jerky" flow behavior while the stress–strain curves for larger samples are relatively smooth, consistent with experiment [31,32]. The evolving dislocation densities for differently sized pillars have also been calculated and are plotted against strain in Fig. 3A–D. Interestingly, the dislocation density for the largest diameter sample (1 μm) increases continuously, while the dislocation density for the smallest sample (150 nm diameter) shows significant fluctuation but overall remains roughly constant with increasing plastic deformation. Supplementary Movies 2A and 2B show the evolution of the dislocation structure, the corresponding stress–strain curves and the evolving dislocation density for both the smallest (150 nm) and the largest (1 μm) diameters, respectively. The colors of the segments indicate the Burgers vectors of the various dislocations, among which the red segments indicate newly created dislocation junctions, formed through reactions of the type $a/2[1\,\bar{1}\,1]+a/2[1\,1\,\bar{1}]=a[1\,0\,0]$, while the green segments indicate glide dislocations with Burgers vectors of the type $a/2\langle 1\,1\,1\rangle$. As shown in Supplementary Movie 2A, dislocations in the smallest pillar escape the pillar so easily that the dislocation density never rises to a high value, with the consequence that few dislocation junctions are formed. On the other hand, as shown in Supplementary Movie 2B, dislocation multiplication is prolific in the largest pillar, spreading dislocations over the entire volume of the cylinder and causing a high density of junctions to form.

To see the size dependence clearly, the flow stresses for a plastic strain of 0.6% were determined and plotted against the corresponding pillar diameters in Fig. 4. To make this plot, we take the flow stresses over seven or nine simulations with random initial conditions for a given sized pillar. The log–log plot gives a size dependence exponent of about −0.48, which is roughly consistent with experimental exponents for bcc metals: −0.24 to −0.48 [28,30,35,36].

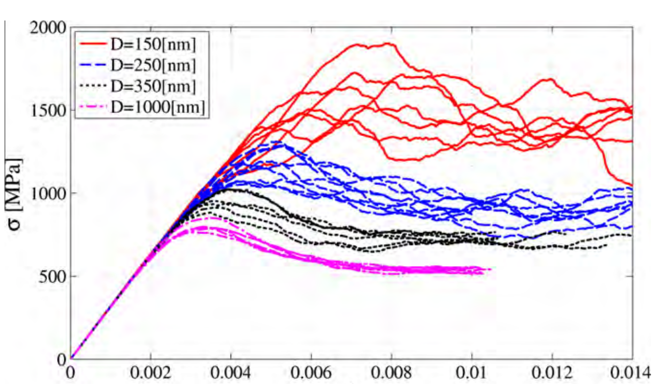

Fig. 2. Stress–strain curves for the 150 nm, 250 nm, 350 nm and 1 μm sized pillars with random initial configurations.

3.2. Effect of initial dislocation density

To study the effect of the initial dislocation density, we have performed simulations with different initial densities ranging from 10^{13} to $8\times10^{13}\ \mathrm{m}^{-2}$. For these simulations, a constant strain rate of $10^{5}\ \mathrm{s}^{-1}$ was imposed and the pillar diameter was 150 nm. Stress–strain curves for three different initial dislocation densities are shown in Fig. 5. We see that the flow stress decreases with increasing initial dislocation density, which is not consistent with the Taylor hardening relationship. However, it can be understood by the fact that the higher dislocation density would result in a softer response by increasing the plastic strain rate, through the Orowan formula, and consequentially decreasing the flow stress rate. These results suggest that Taylor hardening effects are smaller than the softening effects of dislocations as carriers of plasticity.

These results are in good agreement with the microcompression experiments of Bei et al. on Mo pillars [37], wherein pre-straining results in a softer response. Because more highly pre-strained pillars would be expected to have a higher initial dislocation density, the inverse proportionality between initial density and the flow stress predicted by the DD simulation is in accord with experimental results.

3.3. Effect of strain rate

We have also performed simulations for different high strain rates, ranging from 10^{5} to $10^{6}\ \mathrm{s}^{-1}$. Here, the initial dislocation density is again taken to be $10^{13}\ \mathrm{m}^{-2}$ and the pillar diameter is 150 nm. The stress–strain curves for different strain rates are plotted in Fig. 6. At the initial stage of loading, the pillar subjected to a higher strain rate starts to deform plastically at a higher stress (strain), so that the yield stress increases with increasing strain rate. However, the steady-state flow stresses all converged to about 1.6 GPa after around 1.5% strain. As a result, the DD model shows a rate-insensitive steady-state flow stress. However, it must be repeated that the strain rates for the simulations are much higher than those used in experiments, so that a direct comparison with experiments is not yet possible.

4. Dislocation kinetics model for micropillar plasticity controlled by self-multiplication

In an effort to better understand plasticity controlled by the surface cross-slip mechanism, we have developed a simple dislocation kinetics model similar to the one suggested by Nix and Lee [38] for the case of surface nucleation controlled plasticity. A basic assumption of this model is that a fraction of dislocations will self-multiply after it has traveled a distance ℓ, which is approximated by the diameter of a curved dislocation segment under the given stress.

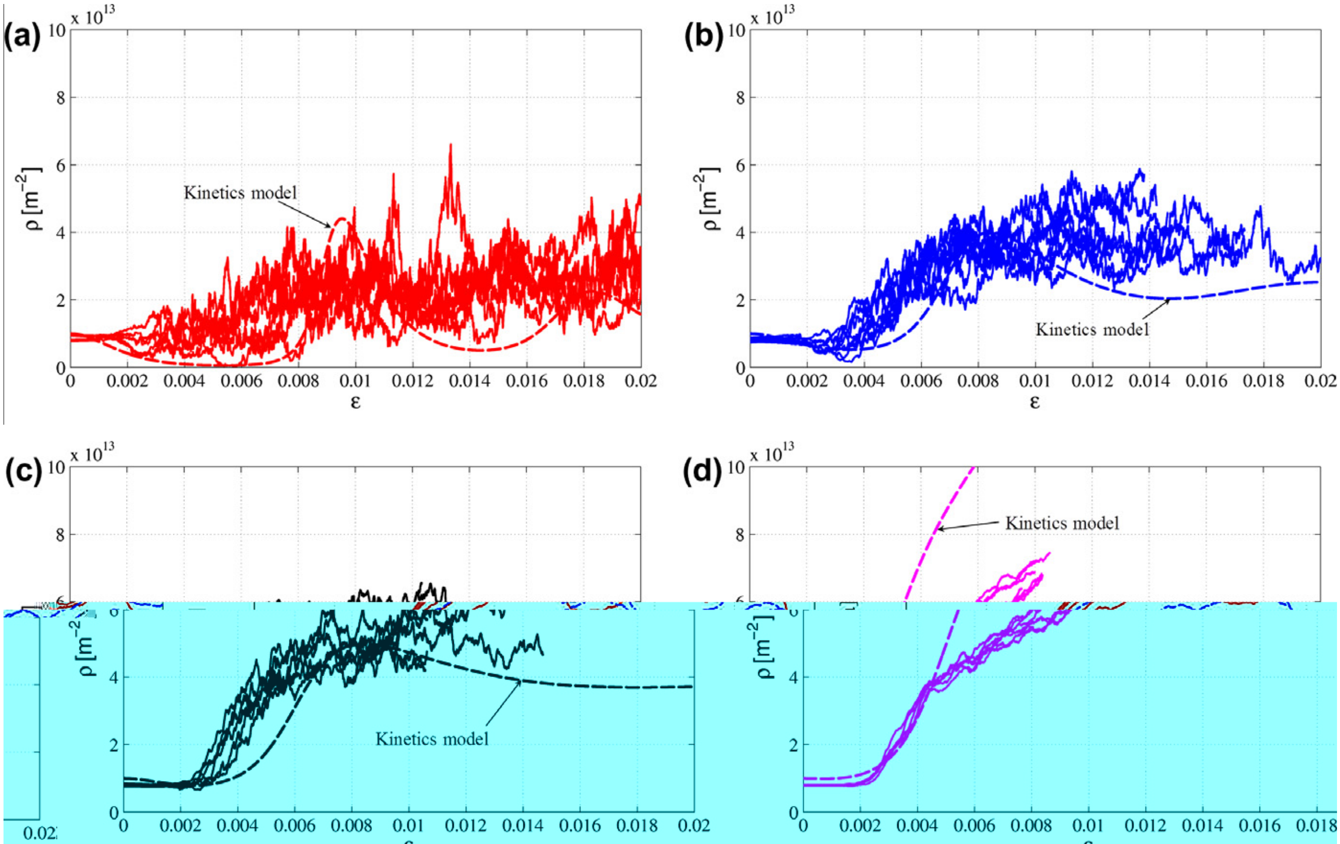

Fig. 3. Dislocation density evolution for the (a) 150 nm, (b) 250 nm, (c) 350 nm and (d) 1 μm sized pillars from DD simulation (solid lines) and the kinetics model (dashed lines).

Fig. 4. Stress at 0.6% plastic strain as a function of pillar diameter. The table shows the average stress among 7–9 DD models with corresponding sized pillars.

Fig. 5. Stress–strain curves with various initial dislocation densities (10^{13}, 4×10^{13} and 8×10^{13} m^{-2}).

The dislocation density is naturally controlled by the competition between the multiplication rate from the surface cross-slip mechanism and the depletion rate associated with dislocations moving out of the surface. Thus the density evolution can be expressed by

$$\dot{\rho} = \dot{\rho}_+ + \dot{\rho}_- \qquad (1)$$

where $\dot{\rho}_+$ stands for the multiplication rate and $\dot{\rho}_-$ is the depletion rate. Adapting the expression for $\dot{\rho}_-$ given by Nix and Lee [38], $\dot{\rho}_-$ may be approximated by the current dislocation density divided by the lifetime of the dislocation, $t_{life} = D/\bar{v}$, where D is the diameter of the sample and $\bar{v}$ is the average velocity of dislocations. Using a linear mobility law, the dislocation depletion rate is

$$\dot{\rho}_- = -\beta \frac{\rho}{t_{life}} = -\beta\rho\frac{M\tau b}{D} = -\beta'\rho\frac{M\sigma b}{D} \qquad (2)$$

where ρ is the current dislocation density, σ the stress along the loading axis and β and β' are constants.

For the multiplication rate, we take the frequency of the dislocation multiplication to be approximated by the aver-

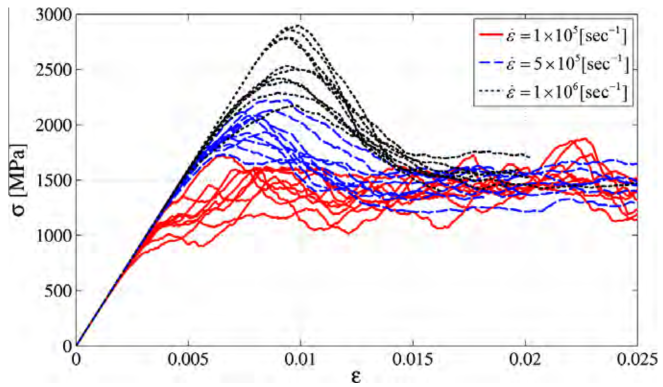

Fig. 6. Stress–strain curves with various strain rates (1×10^5, 5×10^5 and $1 \times 10^6\ s^{-1}$).

age velocity of the screw dislocation divided by the size of the dislocation loop that can be supported by the given stress. Using the expression for the critical bowing stress for a Frank–Read source, the size of the loop can be approximated by

$$\ell = \frac{\mu b}{\tau} \tag{3}$$

where τ is the resolved shear stress. For simplicity, we omit the logarithmic term usually included in this relation. Together with a linear mobility law, the multiplication rate can then be expressed by

$$\dot{\rho}_+ = \alpha\rho\frac{\bar{v}}{\ell} = \frac{\alpha\rho M\tau^2}{\mu} = \frac{\alpha'\rho M\sigma^2}{E} \tag{4}$$

where E is the elastic modulus and α, α' are constants which describe the fraction of dislocations which will self-multiply. Then the dislocation density evolution law is

$$\dot{\rho} = \dot{\rho}_+ + \dot{\rho}_- = \rho M\left(\alpha'\frac{\sigma^2}{E} - \beta'\frac{\sigma b}{D}\right) \tag{5}$$

To compare the dislocation kinetics model with our DD simulations, a constant strain rate needs to be imposed. Thus, the axial stress can be computed as follows:

$$\dot{\sigma} = E(\dot{\varepsilon}^{applied} - \dot{\varepsilon}^{pl}) \tag{6}$$

Using Orowan's formula for the plastic strain rate and a linear mobility law, the resolved shear stress is then

$$\tau = \frac{\dot{\bar{\varepsilon}}^{pl}}{\rho b^2 M} \tag{7}$$

where $\dot{\bar{\varepsilon}}^{pl}$ is the shear strain rate. Considering the Taylor hardening effect, we modified the expression for the resolved flow stress as follows:

$$\tau = \frac{\dot{\bar{\varepsilon}}^{pl}}{\rho b^2 M} + \gamma\mu b\sqrt{\rho} \tag{8}$$

where γ is the Taylor hardening coefficient. Finally, the rate of change in the stress is then

$$\begin{aligned}\dot{\sigma} &= E(\dot{\varepsilon}^{applied} - S\dot{\bar{\varepsilon}}^{pl}) \\ &= E\left[\dot{\varepsilon}^{applied} - S\rho b^2 M(\sigma S - \gamma\mu b\sqrt{\rho})\right]\end{aligned} \tag{9}$$

where S is the Schmid factor in the typical bcc slip system.

To assess the validity of the dislocation kinetics model, the dislocation density (Eq. (5)) and the stress (Eq. (9)) were numerically solved and are plotted in Figs. 7 and 8. For comparison, DD simulation results were also plotted as shaded bands. For the plot, α', β' and γ are chosen to be 0.096, 0.264 and 0.3 respectively, and M is set to be four times higher than the pure screw mobility in the DD model. In Fig. 7, in order to check if the size effect could be predicted by the kinetics model, the diameter varies from 150 nm to 1 μm, with a constant strain rate of $10^5\ s^{-1}$ and an initial dislocation density of $10^{13}\ m^{-2}$, which are the same conditions used for the DD simulations. The kinetics model clearly shows the size effect on the flow stress: as the sample size decreases, the flow stress increases. Moreover, flow stresses and dislocation densities of various sized pillars are within the range of the DD simulation results, as shown in Figs. 3 and 7.According to the kinetics model, without Taylor hardening both the flow stress and the dislocation density eventually reach steady-state values. By setting $\dot{\rho}$, $\dot{\sigma}$ and γ equal to zero, steady-state values of ρ_{SS} and σ_{SS} are found as follows.

$$\sigma_{SS} = \frac{\beta'}{\alpha'}\frac{Eb}{D} \tag{10}$$

$$\rho_{SS} = \frac{\alpha'}{\beta'}\frac{\dot{\varepsilon}^{applied}D}{S^2 b^3 ME} \tag{11}$$

These steady-state values for the stress are plotted for each pillar diameter as horizontal dashed lines in Figs. 7 and 8. The stress–strain curves from the kinetics model with Taylor hardening converge to these steady-state values asymptotically, except for the largest pillar, where Taylor hardening becomes significant. The contribution of Taylor hardening for the largest pillar is to be expected from the sharp increase in the dislocation density for that pillar, as shown in Fig. 3D.

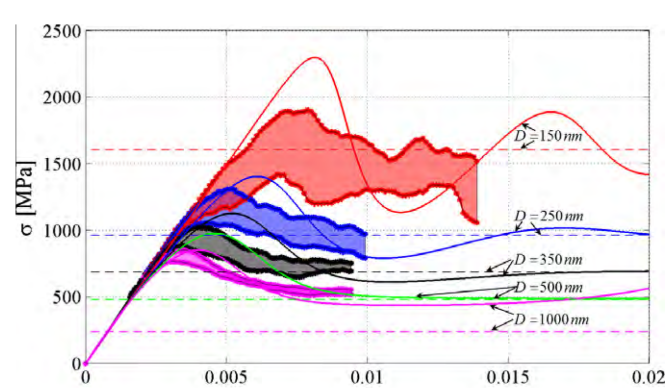

Fig. 7. Numerically solved stress–strain curves from the kinetics model with various sized pillars (150 nm, 250 nm, 350 nm, 500 nm and 1 μm) (solid lines). The steady-state values without hardening effect are plotted in dashed lines. The banded plot corresponds to the DD simulation results for different sized pillars.

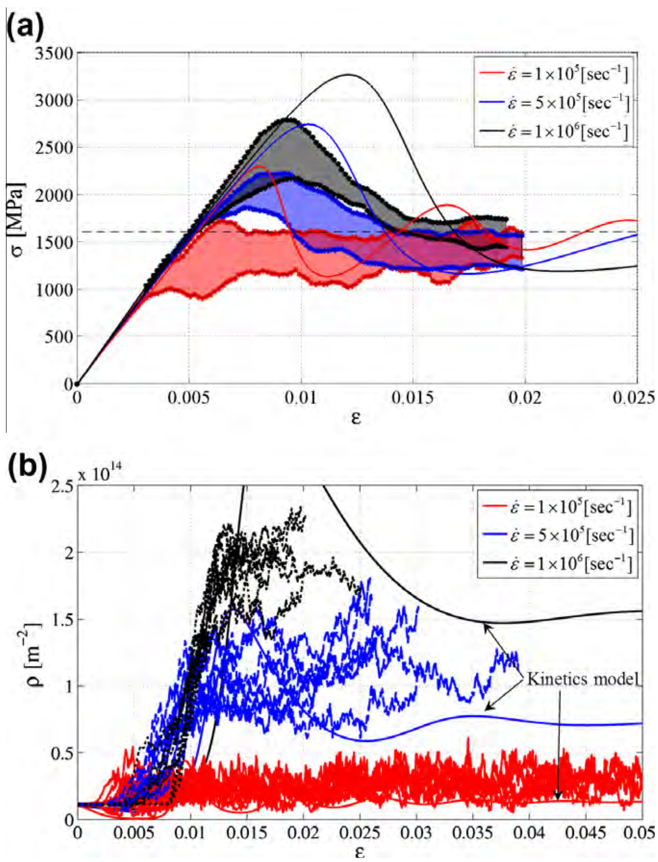

Fig. 8. (a) Numerically solved stress–strain curves (solid line) from the kinetics model with various strain rate (1×10^5, 5×10^5 and 1×10^6 s^{-1}). The steady-state value without hardening effect is plotted in dashed lines. The banded plot corresponds to the DD simulation results for different sized pillars. (b) Dislocation density–strain curves (solid lines). DD simulation results are plotted in red (1×10^5 s^{-1}), blue (5×10^5 s^{-1}) and black (10^6 s^{-1}) lines. (For interpretation of the references to color in this figure legend, the reader is referred to the web version of this article.)

In addition to the size effect, the kinetics model clearly shows a rate insensitivity of the steady-state flow stress, similar to the DD simulations, as shown in Fig. 8A. That is to say, the steady-state flow stress, as predicted by the DD simulations, is independent of the strain rate. As a consequence, the dislocation density remains roughly constant within the range of the DD simulations during further deformation, as shown in Fig. 8B.

5. Discussion

In bulk fcc metals, plastic flow is strongly influenced by junction formation through the elastic interactions of dislocations. The critical stress to bow dislocations between obstacles often plays a dominant role in plastic flow and hardening. Dislocations are assumed to glide quickly from one obstacle to the next so that the kinetics of dislocation motion plays a relatively minor role. By contrast, for the bcc micropillars studied here, the results of the DD simulations as well as the predictions of the kinetics model suggest that at the high strain rates being considered, the size effect on the flow stress arises mainly from dislocation mobility and mobile dislocation density effects. This is also indicated by the simulations, which show that the yield stress decreases with increasing initial dislocation density. This is broadly consistent with the findings of Bei et al. [37], who showed that pre-straining of Mo alloy pillars leads to softening. Consistent with this picture, both the DD simulations and the kinetics model show a strain softening effect associated with the multiplication of dislocations. This is reminiscent of the kind of plastic flow studied by Johnston and Gilman [39]. Thus, neither the dislocation starvation/nucleation model nor the single-arm source model provides a good account of the size dependence of the strength of bcc micropillars at the high strain rates under this study.

The conclusion that the single-arm source model does not describe the simulated flow behavior well might seem to be at odds with some of the features included in the modeling. In both the DD simulations and the kinetics modeling, Orowan bowing effects, with lengths that scale with the size of the pillars, play a key role. In particular, a critical stress for multiplication, which depends inversely on the pillar diameter, is a central feature of this modeling. This might seem to be identical to the single-arm source model wherein the strength of the micropillar is directly related to the critical stress needed to bow a dislocation segment with a length that scales with the pillar diameter. However, in the present modeling, critical stress does not determine the flow stress directly. Rather, it controls the flow stress indirectly through the multiplication of dislocations. In spite of this indirect relation, the steady-state flow stress predicted by the kinetics model (Eq. (10) – without strain hardening) still takes a form that is reminiscent of the predictions of the single-arm source model. The finding that the yield stress of the simulated micropillars increases dramatically with decreasing initial dislocation density (Fig. 5) is the best way to see this distinction. If the single-arm source model were controlling the strength directly, the yield strength would not be expected to increase so dramatically with decreasing initial dislocation density.

As shown in Fig. 8A, both the DD model and the kinetics model predict a strong strain rate sensitivity of the yield stress. This is broadly consistent with experiment, as recent microcompression experiments on sub-micron Mo pillars [27] have shown the flow stress to be strain rate sensitive. However, the rate sensitivity of the yield stress in the present modeling is greater than that observed in the experiments. This is caused by the very high strain rates in the present simulations and the associated linear mobility law we have used. At larger plastic strains the predicted flow stresses for different strain rates tend to converge and lead to a smaller strain rate sensitivity. Eventually, at least for the case of no Taylor hardening, steady-state flow conditions are predicted, wherein the steady-state flow stress is completely independent of strain rate. This is caused by the fact that the steady-state flow stress is completely determined by the competition between a stress-dependent multiplication rate and a stress-independent loss rate. Thus the steady-state flow stress and associated velocity become independent of the strain rate, making the dislocation density directly proportional to the strain rate though the Orowan relation. In the presence of Taylor hardening, such steady states are not predicted. Finally, we note that the compression experiments on sub-micron Mo pillars [27] were conducted under load-controlled conditions. Under these conditions, the strain softening effects shown in the modeling and which eventually lead to steady states could not have been observed. Once strain softening begins, a plateau in the load-controlled stress–strain curve would be observed. The flow stresses reported in Ref. [27] should then correspond to the peak stresses in the simulated stress–strain curves, which do show a strong strain rate sensitivity.

Most existing DD simulations use a simple linear mobility law, in which the velocity of the dislocation segment is proportional to the resolved stress. However, in bcc metals, it is known that the velocity of a screw dislocation is not linearly proportional to the resolved stress due to lattice resistance [40]. Since screw dislocation motion could play an important role in plasticity of bcc metals, it would be useful to modify the mobility law using empirical forms [41,42]. With a nonlinear mobility law, a smaller size dependence exponent might be expected for lower, more realistic strain rates, based on the findings of Lee and Nix [43]. They showed that smaller exponents are expected when the size-independent friction stress is large compared to the flow stress. Further work is needed to account for nonlinear mobility behavior, especially at low stresses in bcc metals.

In the DD simulations, dislocation multiplication occurs intermittently so that the dislocation density shows high fluctuations. This stochastic flow behavior is especially pronounced in the smallest pillars. Since the kinetics model is based on the collective behavior of dislocations, this kind of "jerky" flow behavior cannot be predicted, so that the dislocation density in the kinetics model evolves smoothly, as shown in Figs. 7 and 8. In the DD simulations, the frequency of the fluctuation in the dislocation density is very high, especially for the smallest pillars. Because there is no direct link between the dislocation density and the flow stress, as in the simple kinetics model, the flow stress in the DD simulations is not as sensitive to those abrupt changes in dislocation density. As a consequence, the predicted flow stress in the kinetics model, where there is a direct link between the flow stress and the dislocation density, shows much higher oscillations than those found in the DD simulations, as seen in Figs. 7 and 8. As we have pointed out several times, the present modeling of plasticity of bcc micropillars is limited in the sense that it applies to very high strain rates, much higher than those used in experiments. Further work is needed to extend this analysis to experimental strain rates.

6. Conclusions

In this research, three-dimensional DD simulations have been performed in order to investigate the effects of sample size, initial dislocation density and strain rate on the stress–strain relations of bcc sub-micron metal pillars under uniaxial loading. The DD simulations including a surface cross-slip multiplication mechanism show that the flow stress increases with decreasing pillar size, decreasing initial dislocation density. They also show that yield stress is strongly strain rate sensitive. These findings lead us to the notion that, at the high strain rates considered, plasticity is governed mainly by dislocation mobility and mobile dislocation density effects, not their elastic interactions. We also develop a dislocation kinetics model, based on the competition between multiplication due to the surface cross-slip mechanism and depletion by glide out of the micropillar. Results from both the DD model and kinetics model are in good agreement with recent experiments in bcc metal pillars.

Acknowledgements

Support of this work by the Office of Science, Office of Basic Energy Sciences, of the US Department of Energy under Contract No. DE-FG02-04ER46163 in gratefully acknowledged. This work is partially supported by the NSF Career Grant CMS-0547681. We would like to thank Dr. S.W. Lee of California Institute of Technology for useful discussions.

Appendix A. Supplementary material

Supplementary data associated with this article can be found, in the online version, at http://dx.doi.org/10.1016/j.actamat.2013.02.011.

References

[1] Uchic MD, Dimiduk DM, Florando JN, Nix WD. Science 2004;305:986.
[2] Greer JR, Oliver WC, Nix WD. Acta Mater 2005;53:1821.
[3] Volkert CA, Lilleodden ET. Philos Mag 2006;86:5567.
[4] Fleck NA, Muller GM, Ashby MF, Hutchinson JW. Acta Metall Mater 1994;42:475.
[5] Nix WD, Gao H. J Mech Phys Solids 1998;46:411.
[6] Kraft O, Gruber P, Monig R, Weygand D. Annual Rev Mater Res 2010;40:293.
[7] Greer JR, De Hosson JTM. Prog Mater Sci 2011;56:654.
[8] Greer JR, Nix WD. Phys Rev B 2006;73:245410.
[9] Shan ZW, Mishra RK, Asif SAS, Warren OL, Minor AM. Nat Mater 2008;7:115.
[10] Parthasarathy TA, Rao SI, Dimiduk DM, Uchic MD, Trinkle DR. Scr Mater 2007;56:313.
[11] Rao SI, Dimiduk DM, Parthasarathy TA, Uchic MD, Tang M, Woodward C. Acta Mater 2008;56:3245.
[12] Rao SI, Dimiduk DM, Tang M, Parthasarathy TA, Uchic MD, Woodward C. Philos Mag 2007;87:4777.
[13] Oh SH, Legros M, Kiener D, Dehm G. Nat Mater 2009;8:95.
[14] Kiener D, Minor AM. Nano Lett 2011;11:3816.

[15] Williams DB, Carter CB. Transmission electron microscopy: a textbook for materials science. New York: Plenum Press; 1996.
[16] Devincre B, Kubin LP. Mater Sci Eng A 1997;234–236:8.
[17] Schwarz KW. J Appl Phys 1999;85:120.
[18] Arsenlis A, Cai W, Tang M, Rhee M, Oppelstrup T, Hommes G, et al. Model Simul Mater Sci Eng 2007;15:553.
[19] Espinosa HD, Panico M, Berbenni S, Schwarz KW. Int J Plast 2006;22:2091.
[20] Tang H, Schwarz KW, Espinosa HD. Phys Rev Lett 2008;100:185503.
[21] El-Awady JA, Wen M, Ghoniem NM. J Mech Phys Solids 2009;57:32.
[22] Liu ZL, Liu XM, Zhuang Z, You XC. Scr Mater 2009;60:594.
[23] Motz C, Weygand D, Senger J, Gumbsch P. Acta Mater 2009;57:1744.
[24] Senger J, Weygand D, Motz C, Gumbsch P, Kraft O. Philos Mag 2010;90:617.
[25] Cai W, Bulatov VV. Mater Sci Eng A 2004;387:277.
[26] Brinckmann S, Kim JY, Greer JR. Phys Rev Lett 2008;100:155502.
[27] Schneider AS, Clark BG, Frick CP, Gruber PA, Arzt E. Mater Sci Eng A 2009;508:241.
[28] Schneider AS, Kaufmann D, Clark BG, Frick CP, Gruber PA, Monig R, et al. Phys Rev Lett 2009;103:105501.
[29] Weinberger CR, Cai W. Proc Natl Acad Sci 2008;105:14304.
[30] Greer JR, Weinberger CR, Cai W. Mater Sci Eng A 2008;493:21.
[31] Chisholm C, Bei H, Lowry MB, Oh J, Asif SAS, Warren OL, et al. Acta Mater 2012;60:2258.
[32] Huang L, Li QJ, Shan ZW, Li J, Sun J, Ma E. Nat Commun 2011;2:547.
[33] Weinberger CR, Cai W. J Mech Phys Solids 2007;55:2027.
[34] Weinberger CR, Cai W. Scr Mater 2011;64:529.
[35] Kim JY, Greer JR. Acta Mater 2009;57:5245.
[36] Kim JY, Jang D, Greer JR. Acta Mater 2010;58:2355.
[37] Bei H, Shim S, Pharr GM, George EP. Acta Mater 2008;56:4762.
[38] Nix WD, Lee SW. Philos Mag 2010;91:1084.
[39] Johnston WG, Gilman JJ. J Appl Phys 1959;30:129.
[40] Gilbert MP, Queyreau S, Marian J. Phys Rev B 2011;84:174103.
[41] Gilman JJ. Aust J Phys 1960;13:327.
[42] Prekel HL, Lawley A, Conrad H. Acta Metall Mater 1968;16:337.
[43] Lee SW, Nix WD. Philos Mag 2011;92:1238.